Dynamic performance of biomass based carbons for CO_2/CH_4 separation. Approximation to a PSA process for biogas upgrading.

*Noelia Álvarez-Gutiérrez, Susana García†, María Victoria Gil, Fernando Rubiera, Covadonga Pevida**

Instituto Nacional del Carbón, INCAR-CSIC. Apartado 73, 33080 Oviedo, Spain.

†currently at Centre for Innovation in Carbon Capture and Storage (CICCS), School of Engineering and Physical Sciences, Heriot-Watt University, Edinburgh EH14 4AS, United Kingdom

KEYWORDS. Adsorption; CO_2/CH_4 separation; biomass based activated carbon; breakthrough tests.

ABSTRACT

Physical adsorption based processes such as pressure swing adsorption (PSA) constitute an alternative to selectively adsorb CO_2 from biogas streams. There is abundant work regarding the equilibrium of adsorption of pure CH_4 and CO_2 on different adsorbents. However, to design

an adsorption process with a selected adsorbent it is very important to account for its dynamic behavior in a packed-bed. Thus, the performance of two biomass based activated carbons (CS-CO_2 and CS-H_2O) previously prepared in our laboratory, to separate CO_2/CH_4 has been evaluated. Full adsorption-desorption cycles were conducted at 30 ºC (isothermal conditions) and different pressures (1, 3, 5, and 10 bar) feeding binary CO_2/CH_4 (50/50 vol. %) mixtures to a purpose-built fixed-bed set-up. A commercial activated carbon, Calgon BPL, was also evaluated for reference purposes. CO_2 equilibrium uptakes were obtained from dynamic breakthrough curves and proved to be maxima at 10 bar (5.14, 4.48 and 4.14 mol kg^{-1} for CS-CO_2, CS-H_2O and Calgon BPL, respectively). However the CO_2/CH_4 separation efficiency, according to the difference in breakthrough times between CH_4 and CO_2, is very limited at 10 bar. A combined analysis of the productivity and purity of CH_4 along with CO_2 working capacity derived from dynamic experiments indicates that our biomass based activated carbons would be better candidate materials for the CO_2/CH_4 separation at a pressure of 5 bar than the commercial activated carbon Calgon BPL.

INTRODUCTION

The European Union passed the Directive on Renewable Energy on December 9th, 2009 as part of the EU-Climate Change and Energy Strategy. The directive establishes an overall policy for the production and promotion of energy from renewable sources in the EU with the aim of fulfilling at least 20% of its total energy needs with renewables by 2020. It specifies national renewable energy targets for each country, taking into account its starting point and overall potential for renewables. These targets range from values as low as 10% for Malta to values as high as 49% for Sweden[1]. Therefore, biogas demand is expected to increase

continuously in the coming years because of its ability to produce lower CO_2 emissions than fossil fuels. In addition, the global capacity for power generation from commercial biogas facilities will more than double over the next decade, from 14.5 GW in 2012 to 29.5 GW in 2022[2].

Since biogas contains significant amount of CO_2 (30-65%) [3] its heating value is very low compared to natural gas. Upon removal of water (vapor), hydrogen sulphide, siloxanes, hydrocarbons, ammonia and dust particles, biogas calorific value and relative density need to be adjusted in order to meet the specifications of the Wobbe Index [4], i.e., biogas upgrade to natural gas quality. Towards that purpose and also to avoid pipeline and equipment corrosion, the CO_2 content for pipeline grade bio-methane should be less than 2-3% [5]. On the economical side, the removal of CO_2 is the most critical step in biogas upgrading. The upgrading of biogas takes between 3-6% of the energy of biogas and may cost up to 10 €/GJ for small streams [6].

Currently, several methods are commercially available for the removal of carbon dioxide and other gases from biogas. These methods include adsorption [7], absorption [8] , membranes [9], and cryogenic separation [10]. Among these methods, pressure swing adsorption (PSA) processes have become increasingly competitive.

Biogas is usually delivered at low pressure so it needs to be compressed to a pressure between 4-10 bar before the PSA unit [11]. The main goal of the PSA process is to produce fuel grade methane (methane purity $\geq$ 97%) [12]. It is however most likely that in the future more stringent specifications will apply to the methane recovery given its high Global Warming Potential [13, 14]. The PSA process relies on the fact that under pressure, gases tend to be attracted to solid surfaces, or "adsorbed". The higher the pressure, the more gas is adsorbed; when the pressure is reduced, the gas is released, or desorbed. Despite the remarkable growth in practical

64 applications of adsorptive gas separation processes, their commercial design and optimization
65 still require a significant experimental effort.

66 After original work by Sircar in the late 1980s [15], many studies have been performed on
67 PSA processes aimed at separating CO_2 from gaseous streams containing CH_4 [16-21]. Most studies
68 have focused on zeolites [22-24], metal-organic frameworks [14, 25-27], and activated carbons [28-30].

69 Knowledge of the dynamic fixed-bed behavior is an elemental tool to validate the model
70 used to describe the PSA performance [31]. Literature on the dynamic performance of adsorbent
71 beds for CO_2/CH_4 separation is scarce [32-34] and specific data on biomass based activated carbons
72 for biogas upgrading under similar operational conditions to those presented here is lacking.

73 Two biomass based activated carbons (CS-CO_2 and CS-H_2O) previously prepared in our
74 laboratory have shown great potential for the above application based on their CO_2 and CH_4
75 equilibrium capture capacities (static) at high pressures [35]. However, as previously mentioned,
76 the dynamic fixed-bed behavior is required to ascertain the extent to which the equilibrium
77 uptake may be translated into breakthrough capacity. In this work, the performance of these
78 biomass based materials has been evaluated under dynamic conditions. Hence, breakthrough
79 experiments were performed with a simulated binary gas stream consisting of CO_2 and CH_4
80 (50/50 vol. %) at 30 ºC and varying total pressures (1, 3, 5, and 10 bar). A commercial activated
81 carbon, Calgon BPL, was also evaluated for comparison purposes.

82 Finally, the performance of the tested adsorbents over consecutive adsorption-desorption
83 long cycles (120 to 300 min) has been used to evaluate a set of parameters for the design and
84 optimization of a PSA process applied to biogas upgrading.

85

MATERIALS AND METHODS

Materials

Two biomass-based activated carbon samples (CS-CO_2 and CS-H_2O) previously prepared in our laboratory from cherry stones, a low cost biomass residue from the Spanish food industry, have been evaluated as adsorbent materials. CS-CO_2 and CS-H_2O samples were activated in a CO_2 and H_2O single-step process, respectively. A fully detailed chemical and textural characterization of these carbons has been reported previously[36]. Moreover, in this study, a commercial activated carbon, Calgon BPL, was chosen for comparison purposes. Details on its chemical and textural characterization can be found elsewhere [37]. All gases used in this work were obtained from Air Products with purities higher than 99.995%. Table 1 summarizes the main characteristics of the evaluated adsorbents.

Static measurements

CO_2 and CH_4 adsorption isotherms at 30 ºC and up to 10 bar were determined in a high pressure magnetic suspension balance, Rubotherm-VTI. The initial mass of sample used for the adsorption isotherms was approximately 0.5 g and the equilibrium criteria was set to 0.0050 wt% change in 10 min. Prior to adsorption, the sample was dried in situ under vacuum at 100 ˚C for 120 min. The cell holding the sample is then cooled down to the measuring temperature, and pressurization is attained with the desired adsorbate in a stepwise mode, so the change in the weight of the adsorbent sample as well as pressure and temperature are measured and recorded when equilibrium is reached.

Experiments with helium were carried out in order to determine the volume of the adsorbent and cell system, enabling the effect of buoyancy on the measurements to be evaluated.

The absolute amount of CO_2 and CH_4 adsorbed over the pressure range tested were estimated following the procedure described in a previous work [38].

Dynamic column breakthrough measurements

Experimental set up. All experiments were conducted in a lab-scale fixed-bed reactor packed with the adsorbent material. The main characteristics of the adsorbent beds are summarized in Table 2. It is worth pointing out that almost double amount of BPL activated carbon sample (7 g) was required for the experimental runs when compared to the biomass-based samples (4.1 g of CS-CO_2 and 4.8 g of CS-H_2O), which was derived from targeting a similar bed height in all the experiments.

The detailed description of the system can be found elsewhere [39]. The stainless steel fixed-bed reactor is 13.3 cm in height, 1.3 cm in diameter and is equipped with a porous plate located 4.7 cm from the base of the column. The gas manifold system consists of three lines fitted with mass flow controllers from Bronkhorst High-Tech with flows ranging between 1 and 200 mL min^{-1} STP. The controllers have an accuracy of 1% full scale and a repeatability of 0.1% full scale. One of the lines is used to feed in an inert gas, He, in order to dry the sample before each experiment. The other two lines feed in CO_2 and CH_4. To monitor the column temperature a K-type thermocouple with an accuracy of ±1.5 ºC was used, which is located at a height of 3.6 cm above the porous plate (exit end of the column). The mass flow rate of the effluent from the adsorbent bed was measured using a mini CORI-FLOW meter from Bronkhorst. Effluent gas analysis was performed by means of a dual channel micro-gas chromatograph, Varian CP-4900, fitted with a thermal conductivity detector (TCD) in which He and Ar were used as the carrier gases.

130 *Breakthrough tests*. Prior to each experiment, the TCD was calibrated employing
131 CO_2/CH_4/He mixtures of known compositions. The bed was packed with activated carbon in
132 order to measure the dynamics of the CO_2 and CH_4 in the column. A simulated biogas CO_2/CH_4
133 mixture (50/50 vol. %) was fed (30 mL min^{-1} STP) to the adsorption unit and the adsorption
134 performance of the samples was evaluated at a temperature of 30 ºC under isothermal conditions
135 and four different pressures (1, 3, 5, and 10 bar). For each sample six consecutive adsorption-
136 desorption cycles were conducted to test the reproducibility of the system, where adsorption
137 proceeded until saturation and desorption was extended to full regeneration of the activated
138 carbon samples.

139 Each experimental run involved the following steps: (i) drying of the adsorbent before
140 each experiment by flowing He (50 mL min^{-1} STP) for 60 min at 180 ºC and atmospheric
141 pressure, (ii) pressurization and cooling down to the adsorption temperature (30 ºC) in a
142 preconditioning step of 20 min, where 50 mL min^{-1} (STP) of He was allowed to flow through the
143 system, (iii) feed gas switch to a CO_2/CH_4 gas mixture for a duration of 60 min (120-180 min for
144 the experiments at 10 bar) so adsorption takes place until complete saturation is achieved, and
145 (iv) depressurization of the unit and atmospheric pressure purge with 50 mL min^{-1} (STP) of He
146 at 180 ºC for 60 min (120 min for experiment at 10 bar) to fully desorb the adsorptive gases from
147 the column. During the adsorption stage the CO_2 and CH_4 concentrations in the column effluent
148 gas were continuously monitored as a function of time -breakthrough curve- and maximum or
149 equilibrium dynamic adsorption capacity of the adsorbents were calculated after the outlet CO_2
150 concentration equaled that of the inlet stream. However, in a typical operation, the flow would be
151 stopped or diverted to a fresh adsorbent bed once the CO_2 concentration reached that limit [40].

The equilibrium CO_2 adsorption capacity and breakthrough time, t_b, or time it takes for CO_2 to be detected at the adsorption column outlet, were calculated as an average of values obtained from six consecutive adsorption-desorption cycles. Also, as adsorbents were fully regenerated, the repeatability of breakthrough curves could be assessed. Equilibrium adsorption capacities were determined by applying a mass balance equation to the bed as well as accounting for gas accumulated in intraparticle voids and dead space of the bed [37].

Blank experiments were also conducted at 30 ºC and at the different pressures with a bed packed with glass beads of approximately 3 mm diameter. With these experiments extra-column effects (e.g., gas holdup) during the breakthrough tests at the different pressures could be accounted for.

RESULTS AND DISCUSSION

Breakthrough curves from binary CO_2/CH_4 adsorption experiments

The CO_2 and CH_4 concentration at the outlet of the bed were measured for the adsorbents at the selected adsorption pressures and C/C_0 (ratio between the outlet CO_2 or CH_4 concentration at a given time and that in the feed) was plotted versus time (Figure 1). The breakthrough times were taken at a relative concentration ($C_{i,outlet}/C_{i,feed}$) of 0.05.

It is observed that after an initial period during which both components are fully adsorbed, CH_4 always breaks first and its breakthrough curve exhibits a so-called roll-up or roll-over, which means that the molar flow rate of CH_4 in the effluent is temporarily higher than that fed to the adsorption bed. The explanation for this phenomenon is that CH_4 is first adsorbed and thereby concentrated in the adsorbent, but then it is displaced by CO_2 whose concentration front advances slower through the column than that of CH_4. The so-induced desorption of CH_4 is

175 responsible for a CH_4 flow rate rise above the feed flow rate. As time goes by, the concentration
176 of both components at the outlet evolves to feed concentration level, indicating that the column is
177 saturated. The preferential adsorption of CO_2 over CH_4 can be explained by the different
178 adsorption strength of the two molecules. The permanent quadrupole moment of CO_2 (-1.4×10^{-35} cm)
179 leads to strong adsorption; CH_4, in contrast, is not capable of similar interactions and is
180 therefore adsorbed less strongly [41]. The amplitude of the roll-up is a measure of the competition
181 between CO_2 and CH_4 for adsorption sites: it is high when a large amount of CH_4 is rapidly
182 replaced by incoming CO_2. An adsorbent may be selective because it intrinsically adsorbs very
183 little CH_4 (early breakthrough of CH_4, weak roll-up), strongly prefers CO_2 over CH_4, in spite of a
184 fairly strong interaction with CH_4 (late breakthrough of CH_4, strong roll-up), or by a combination
185 of both effects [42].

186 As shown in Figures 1a to 1c, consecutive breakthrough curves (identified by the same
187 color and different symbols) practically overlap showing that adsorbents were fully regenerated
188 and samples remained stable after six consecutive adsorption-desorption cycles. Based on
189 observed CH_4 and CO_2 concentration fronts, CO_2/CH_4 separation might be feasible on CS-CO_2
190 and CS-H_2O samples as a clear difference in breakthrough time between CO_2 and CH_4 is
191 observed. However, the ability to separate CO_2/CH_4 is reduced for the commercial activated
192 carbon Calgon BPL (Figure 1c) given the closer breakthroughs of CO_2 and CH_4. This indicates
193 that Calgon BPL is less selective than our carbons.

194 It is well known that pressure affects the shape of the breakthrough curve as well as the
195 breakthrough time. Higher adsorption pressures (i.e., higher CO_2 and CH_4 partial pressures) lead
196 to increase adsorbed amounts and so the concentration front of each adsorptive takes more time

197 to reach the bed outlet. For instance, the CO_2 adsorption front reaches the bed outlet after
198 approximately 9 min at 1 bar and after 25 min at 10 bar for carbon CS-CO_2 (see Figure 1a).

199 In Figure 2 the CO_2 and CH_4 breakthrough curves for the activated carbons at each
200 pressure studied (1, 3, 5, and 10 bar) have been overlapped for comparison purposes.

201 The mass-transfer zone (between the break point and saturation) where most of the
202 change in concentration occurs becomes wider with increasing pressure (see Figure 2). For the
203 cherry stones-based carbons this is remarkable only at 10 bar but in the case of Calgon BPL the
204 broadening of the breakthrough curves is also observed at lower pressures. The width and shape
205 of the mass-transfer zone depend on the mass-transfer rate, the flow rate and the shape of the
206 equilibrium adsorption isotherm. Breakthrough curves are usually *S*-shaped due to the role of
207 internal diffusion resistance that tends to increase when the solid becomes nearly saturated.
208 However, if pore diffusion is controlling the rate of adsorption the breakthrough curve has the
209 opposite shape. This could be the case for CO_2 adsorption on Calgon BPL at 5 and 10 bar where
210 concave downwards curves are encountered.

211 In the case of CH_4, the breakthrough curves at the different pressures present similar
212 slopes for the cherry stones activated carbons. It is observed that at 10 bar the height of the roll-
213 up decreases but it becomes broader. Calgon BPL shows a different pattern in the CH_4
214 breakthrough curves: at pressures $\geq$ 5 bar the slopes and the roll-up are remarkably different.

215 Blank experiments with glass beads (non-adsorbent solid) are also included in Figure 2d.
216 As expected breakthrough times are considerably reduced with respect to the adsorption
217 experiments and no roll-up is observed. It can be seen that the sharpness of the curves drastically
218 changes at 10 bar. This could be a result of the volume of gas accumulated in the voids of the

219 bed. At higher pressures the holdup of gas in the bed could be significant relative to the amount
220 adsorbed and this gas volume must be considered in designing the adsorption cycle.

221 The equilibrium adsorption isotherms of CO_2 and CH_4 for the evaluated carbons are
222 plotted in Figure 3 for discussion purposes. Detailed description and discussion of the
223 equilibrium of adsorption of CO_2 and CH_4 on the CS-carbons has been reported elsewhere [35].
224 When adsorption is characterized by linear isotherms broad breakthrough curves are
225 encountered. The CO_2 isotherm of Calgon BPL presents a more linear pattern than the CS-
226 carbons: the CO_2 uptake is below that of the CS-carbons up to pressures of around 6 bar but at
227 higher pressures Calgon BPL exceeds that of CS-H_2O and eventually reaches the uptake of CS-
228 CO_2 at 10 bar. CH_4 adsorption follows a similar pattern for the three carbons.

229 The width of the mass-transfer zone is related to the bed length meaning that very long
230 beds might be required to make the transfer zone a small fraction of the bed in contrast to
231 adsorption with favorable isotherms. A narrow mass-transfer zone is desirable to make efficient
232 use of the adsorbent bed and to reduce the energy cost associated with its subsequent
233 regeneration [43]. In fact, an ideal sorbent would have a vertical breakthrough curve, which would
234 be representative of negligible mass-transfer resistance and minimal axial dispersion.
235 Nevertheless, differentiation between dispersion and mass-transfer coefficients contributions to
236 the spreading breakthrough curves is not straightforward and will require dedicated experiments
237 and detailed modeling calculations.

238 The time elapsed between the CH_4 and the CO_2 breakthrough is indicative of the
239 separation performance of the solids bed: the greater the difference in breakthrough times
240 between both adsorbates, the higher the separation effectiveness. Moreover, it is observed in
241 Figures 1a to 1c that there is a time interval when high purity CH_4 can be recovered at the bed

outlet. Cycle times in a continuous process, such as a PSA process, will be influenced by this breakthrough time difference which, in turn, would affect the amount of pure CH_4 that can be produced per cycle.

The values of the breakthrough time for each sample versus the total pressure have been represented in Figure 4. Little differences are encountered between the biomass based activated carbons and the commercial activated carbon Calgon BPL in the lower pressure range (< 5 bar). At 5 and 10 bar differences between samples become apparent with CS-H_2O showing the longest CO_2 breakthrough times. In terms of CH_4 adsorption, Calgon BPL shows slightly higher breakthrough times at all pressures.

At 10 bar the time lag between the CH_4 and CO_2 breakthrough curves is reduced and a significant amount of CH_4 is co-adsorbed with CO_2 on samples CS-CO_2 and Calgon BPL limiting the separation CO_2/CH_4. Peter et al. studied the dynamic adsorption-desorption behavior of CO_2 and CH_4 in amino-MIL-53(Al) at different temperatures (30, 45 and 60 ºC) and pressures (1, 5 and 30 bar). They also observed that at 30 bar the time lag between the breakthrough curves for both gases decreased significantly with respect to 1 and 5 bar [14].

Therefore, it is inferred from our experimental results that despite the similarities in breakthrough time the samples produced from a biomass waste present potential advantage to separate CO_2/CH_4 mixtures over the commercial activated carbon Calgon BPL.

Equilibrium adsorption capacity from dynamic experiments

The adsorbed amounts of CO_2 and CH_4 calculated from the breakthrough experiments are tabulated in Table 3. The amounts of CO_2 and CH_4 adsorbed at equilibrium were determined as an average of the capture performance of the adsorbents after conducting six consecutive adsorption-desorption cycles. A mass balance equation to the bed was applied to each

265 adsorption-desorption cycle, which considered the gas accumulated in the intraparticle voids and
266 dead spaces of the bed. More details about the calculation procedure can be found in Gil et al. [37,
267 39].

268 While adsorption capacities are usually reported in the literature on a mass basis (e.g. mol
269 of CO_2 adsorbed per kg of adsorbent), the volumetric capacities (e.g. mol of CO_2 adsorbed per
270 m^3 of adsorbent) were also calculated, since both parameters are critical in designing adsorption
271 separation processes [44].

272 The uptakes obtained from the breakthrough experiments indicate that, as expected, the
273 adsorption capacity of the activated carbons increased with pressure. For instance, the capacity
274 values obtained at 30 ºC for the CS-CO_2 sample rose from 1.63 to 5.14 mol kg^{-1} adsorbent as the
275 pressure increased from 1 to 10 bar.

276 The CO_2 adsorption capacity on a mass basis followed the order: CS-CO_2 > CS-H_2O >
277 Calgon BPL (Table 3). The greatest CO_2 adsorption capacity (5.14 mol kg^{-1}) corresponds to the
278 biomass based activated carbon CS-CO_2 at 10 bar. The CH_4 adsorption capacity on a mass basis
279 showed similar trend although the difference among the uptakes of the adsorbents is less
280 noticeable than in the case of the CO_2 adsorption capacity. The greatest CH_4 uptake on a mass
281 basis (1.55 mol kg^{-1}) corresponds to CS-CO_2 at 10 bar.

282 It has been previously reported that at high pressure, the total micropore volume,
283 determined by N_2 adsorption isotherms at -196 ºC, is the textural parameter more directly related
284 to the CO_2 adsorption capacity of the materials [45, 46]. In fact, Wiersum et al. observed that at high
285 pressure the solid with the largest pore volume also exhibited the highest uptakes while the solid
286 with the smallest pore volume adsorbed the least [47]. However, in this work we encounter the
287 opposite trend. Based on textural properties of the materials (Table 1), Calgon BPL is the sample

with largest micropore volume (0.46 cm^3 g^{-1}) compared to CS-CO_2 (0.40 cm^3 g^{-1}) and CS-H_2O (0.38 cm^3 g^{-1}). This may be attributed to the significantly narrower average micropore width of the biomass based carbons (Table 1) that also plays a significant role in high pressure adsorption [46].

Comparing the calculated capacities on a volumetric basis the previous trend is reversed. The CO_2 adsorption capacity follows the order: Calgon BPL > CS-H_2O > CS-CO_2 (Table 3). This is mainly attributed to a different bed weight for breakthrough tests with Calgon BPL (see bed density in Table 2) as a constant bed height was targeted for the experiments with three different adsorbents. This is a disadvantage of the biomass based carbons that could be overcome with tailored conformation during the production process. It should be noted however, that the large CO_2 adsorption capacity on a volumetric basis of Calgon BPL, is also accompanied by significant CH_4 adsorption that may lead to reduce adsorption selectivity.

Optimization of adsorption conditions

Generally, in a PSA process one of the feed components is preferably adsorbed in the bed (in this case CO_2), while the rest of them are weakly adsorbed and leave the bed forming the raffinate. During subsequent regeneration, the CO_2 retained is desorbed and it is recovered as extract. Therefore, the target is to recover most, in this case CO_2, as part of the extract and with the highest possible purity. Nevertheless, in biogas upgrading both raffinate (CH_4) and extract (CO_2) are valuable products that might be recovered at high purity. Therefore, the purity level of the CH_4 will be dictated primarily by the breakthrough of CO_2 that is first eluted from the adsorbent bed.

The dynamic experiments were conducted until saturation and complete regeneration of the solids bed were reached in each cycle. In a real PSA process the feed step is normally

311 terminated before the most strongly adsorbed component breaks through the bed (saturation),
312 while the regeneration step is generally terminated before the bed is fully regenerated.

313 The analysis of transient breakthroughs has proved useful to evaluate the separation
314 performance of adsorbents [48]. By analyzing the performance of these long cycles we can identify
315 conditions that would be feasible in short cyclic experiments to be applied to a real PSA process
316 aimed for biogas upgrading.

317 Therefore, in this work, three different parameters have been selected to account for the
318 process performance. These are: CO_2 working capacity, CH_4 productivity and CH_4 purity. The
319 last one is defined through the operating conditions of the process. As we have mentioned in the
320 Introduction, the present study does not intend to conduct a detailed design and/or optimization
321 of a PSA unit.

322 The working capacity is defined herein as the difference between the loading of the
323 component that needs to be preferentially adsorbed, expressed in moles per kilogram of
324 adsorbent, at the "adsorption" pressure and the corresponding loading at the "desorption", or
325 purge, pressure, here assumed to be 1 bar. The higher the working capacity is, the larger the
326 amount of feed that can be treated with a given amount of adsorbent within a given period of
327 time [3, 49, 50].

328 The amount produced per kg of material or productivity is relevant for grass-roots design
329 of PSA units; this metric is directly a reflection of the adsorbent cost [51].

330 Maximum values of CO_2 working capacity and productivity are desired as a smaller
331 adsorbent bed volume would be then required. Therefore, capital and operating costs would
332 decrease.

In order to determine the pressure level for the adsorption stage, one should keep in mind that the larger the difference between the capacities of the competing adsorbates, the purer the raffinate will be. For a given separation, the product purity is predetermined and the size of the adsorbent bed is inversely proportional to the adsorbent productivity. It is important to keep in mind that these parameters are interrelated for any given PSA process [17].

Design parameters. Discussion and implication for biogas upgrading. As we previously mentioned, one of the parameters that we have taken into account to compare our materials is the working capacity. The experimental working capacity of CO_2 was obtained by calculating the difference between the adsorbed amounts of CO_2 under adsorption and desorption conditions (here assumed to be 1 bar). The calculated values assuming adsorption pressures of 3, 5 and 10 bar are represented in Figure 5. As might be expected working capacity increases with pressure and the highest values for the three adsorbents are obtained at 10 bar. This is in agreement with the equilibrium adsorption capacities from static single component adsorption isotherms (Figure 3) and dynamic binary breakthrough tests (Table 3). At 10 bar it was observed previously that the efficiency of the CO_2/CH_4 separation decreases and a great amount of CH_4 is also co-adsorbed with CO_2. Thus, this may not be the pressure that best suits the adsorption step in this process and it will be discarded in following analysis. On the other hand, it is observed in Figure 5 that the working capacity of Calgon BPL is lower than that of CS-CO_2 and CS-H_2O.

From the data presented in Figures 1a to 1c we can determine the amount of CH_4 in the exit gas stream. As illustration, Figure 6 shows the experimental breakthrough for CO_2/CH_4 mixture (50/50 vol. %) at 30 ºC and at 5 bar in the fixed bed packed with CS-CO_2. The y-axis represents the % CH_4 in the exit gas stream. During the time interval between t_1 and t_2, CH_4 can be produced with a purity of approximately 95%. Thus the productivity of CH_4, with the selected

95% purity level, can be estimated from a material balance by integrating the CH_4 molar flow rate profile in the outlet gas between the time interval t_1 to t_2, as follows:

$$CH_4\ productivity = \frac{1}{m_{ads}\ t}\int_{t_1}^{t_2} F_{CH_4,exit}\,dt \quad (1)$$

where F_{CH4},exit is the molar flow rate of CH_4 that exits the bed, m_{ads} is the mass of adsorbent packed in the bed and t is the time interval (t_2-t_1) when CH_4 leaves the bed at the selected purity (~95%). Productivity, as estimated from Equation 1, is then reported in mol per kg of adsorbent and unit of time.

Figure 7 shows the amount of CH_4 produced in the outlet stream, per kilogram of adsorbent material and minute, versus pressure. There is not a direct correlation between the productivity of CH_4 and total pressure. However, it seems clear that Calgon BPL has significantly lower productivities than our adsorbents. Maximum CH_4 productivity of 0.26 mol kg^{-1} min^{-1} is achieved for CS-CO_2 and CS-H_2O at 3 and 5 bar, respectively.

In Figure 8 the purity of CH_4 in the outlet gas stream is presented as a function of the total pressure in the breakthrough experiments for the three adsorbents. The concentration of CH_4 tends to decrease with increasing pressure and more remarkably for Calgon BPL, where the concentration of CH_4 is below 85% at 5 bar. However, the purity of CH_4 in the outlet stream remains practically constant (~ 95%) for carbon CS-H_2O in the evaluated pressure range.

As mentioned above, maximum values of CO_2 working capacity and CH_4 productivity must be sought since they are closely related to the size of the adsorber. Figure 9 shows CH_4 productivity versus CO_2 working capacity for the studied carbons. As can be observed, CH_4 productivity slightly varies with CO_2 working capacity for each carbon. Thus, maximum CO_2 working capacity turns to be the prevailing criteria. For CS-CO_2, and CS-H_2O this condition is achieved at the maximum pressure of 5 bar at which CO_2/CH_4 separation is still feasible. On the

379 other hand, Calgon BPL shows poor performance in terms of CH_4 productivity and CO_2 working
380 capacity when compared to our biomass based carbons.

381 The experimental results show that at a pressure of 5 bar the performance of CS-H_2O is
382 slightly superior to that of CS-CO_2. Despite the similar adsorption capacities on a mass basis of
383 both CS-carbons, CS-H_2O shows slightly better breakthrough time, CO_2 working capacity and
384 CH_4 productivity and purity. Moreover, it shows enhanced adsorption capacity on a volumetric
385 basis which would allow reduced size of the required equipment.

386 In a previous work [35] we focused on the analysis of the equilibrium of adsorption of CO_2
387 and CH_4 from static gravimetric isotherms up to pressures of 10 bar. Despite the great
388 similarities of both CS-carbons in terms of adsorption capacities we identified CS-CO_2 as
389 preferred adsorbent for the separation of CO_2 from a CO_2/CH_4 mixture representative of a biogas
390 stream. That conclusion was based on the enhanced values of an adsorption performance
391 indicator that accounts for the selectivity, the working capacity and the isosteric heat of
392 adsorption of CO_2. Herein, breakthrough tests were conducted under isothermal operation and so
393 heat effects on the adsorption performance of the adsorbents are deliberately avoided. Therefore,
394 comparison is not straightforward. However, in the aforementioned work it was also clearly
395 concluded that in terms of the selection parameter *S* (that accounts for the ratio of the working
396 capacities of the two gases and the equilibrium selectivity to CO_2), CS-H_2O was slightly superior
397 to CS-CO_2. This is in good agreement with the isothermal breakthrough experiments carried out
398 in this work that also indicate that CS-H_2O presents better performance for biogas upgrading at a
399 pressure of 5 bar.
400

CONCLUSIONS

Analysis of CO_2 and CH_4 co-adsorption on two biomass based activated carbon (CS-CO_2 and CS-H_2O) materials has been performed by means of dynamic breakthrough experiments in a packed-bed. A commercial activated carbon Calgon BPL was also studied for comparison purposes.

The evaluated adsorbents showed good cyclability and regenerability over consecutive adsorption-desorption cycles. CO_2/CH_4 separation is feasible on CS-CO_2 and CS-H_2O according to the difference in breakthrough time between CO_2 and CH_4. However, this ability is reduced for Calgon BPL indicating that it is less selective than our carbons.

The adsorption pressure in a PSA process should be carefully chosen considering the process performance. ~~We have analyzed the purity and productivity of CH_4 and the CO_2 working capacity from binary CO_2/CH_4 equimolar breakthrough tests conducted at 30ºC and varying pressures. When adsorption pressure increases CO_2 working capacities also increase.~~ It is observed that when adsorption pressure increases so does CO_2 working capacity. However, at 10 bar the efficiency of the CO_2/CH_4 separation drastically decreases for the evaluated adsorbents.

CS-CO_2 and CS-H_2O have good adsorption capacities with measured CO_2 working capacities of 1.96 and 2.04 mol kg^{-1} for CS-CO_2 and CS-H_2O, respectively, when adsorbents are cycled between 5 bar of adsorption pressure and 1 bar of regeneration pressure. Maximum CH_4 productivities of 0.26 mol kg^{-1} min^{-1} are achieved for CS-CO_2 and CS-H_2O at 3 and 5 bar, respectively. ~~These values are higher than those of Calgon BPL (working capacity of CO_2 in the same conditions of 1.53 mol kg^{-1} and CH_4 productivity of 0.15 mol kg^{-1} min^{-1} at 3 bar).~~ On the other hand, the purity of CH_4 in the outlet stream for both biomass based activated carbons is above 95%. ~~whereas for Calgon BPL the purity of CH_4 drastically decreases with pressure.~~

These values are higher than those of the commercial Calgon BPL. From the results presented it can be concluded that our biomass based activated carbons, CS-CO_2 and CS-H_2O, are promising adsorbents for CO_2/CH_4 separation operating at a pressure of 5 bar.

AUTHOR INFORMATION

Corresponding Author

*(C.P) Phone: +34 985 11 89 87 / 985 11 90 90 (Ext. 319). Fax: +34 985 29 76 62. Email: cpevida@incar.csic.es.

Author Contributions

The manuscript was written through contributions of all authors. All authors have given approval to the final version of the manuscript.

Funding Sources

Project: ENE2011-23467 (Spanish MINECO) and GRUPIN14-079 Grant (Gobierno del Principado de Asturias, Spain).

ACKNOWLEDGMENT

This work has received financial support from the Spanish MINECO (Project ENE2011-23467), co-financed by the European Regional Development Fund (ERDF), and from the Gobierno del Principado de Asturias (PCTI2013-2017, GRUPIN14-079). N.A-G. also acknowledges a fellowship awarded by the Spanish MINECO (FPI program), and co-financed by the European Social Fund.

REFERENCES

1. Commision, E., Directive 2009/28/EC of the European Parliament and of the Council of 23 April 2009 on the promotion of the use of energy from renewable sources and amending and subsequently repealing Directives 2001/77/EC and 2003/30/EC. In Official Journal of the European Union: 2009.
2. Research, P. Worldwide power generation capacity from biogas will double by 2022. . http://www.businesswire.com/news/home/20121107005284/en/Worldwide-Power-Generation-Capacity-Biogas-Double-2022%20-.U3NpFViSwwk
3. Remy, T.; Gobechiya, E.; Danaci, D.; Peter, S. A.; Xiao, P.; Van Tendeloo, L.; Couck, S.; Shang, J.; Kirschhock, C. E. A.; Singh, R. K.; Martens, J. A.; Baron, G. V.; Webley, P. A.; Denayer, J. F. M., Biogas upgrading through kinetic separation of carbon dioxide and methane over Rb- and Cs-ZK-5 zeolites. *RSC Advances* **2014,** 4, (107), 62511-62524.
4. Ryckebosch, E.; Drouillon, M.; Vervaeren, H., Techniques for transformation of biogas to biomethane. *Biomass and Bioenergy* **2011,** 35, (5), 1633-1645.
5. Delgado, J. A.; Uguina, M. A.; Sotelo, J. L.; Ruíz, B.; Rosário, M., Carbon Dioxide/Methane Separation by Adsorption on Sepiolite. *Journal of Natural Gas Chemistry* **2007,** 16, (3), 235-243.
6. Petersson, A.; Welllinger, A. *Biogas upgrading technologies-developments and innovations*; Task 37 - Energy from biogas and landfill gas: 2009.
7. Sarkar, S. C.; Bose, A., Role of activated carbon pellets in carbon dioxide removal. *Energy Conversion and Management* **1997,** 38, Supplement, S105-S110.
8. Horikawa, M. S.; Rossi, F.; Gimenes, M. L.; Costa, C. M. M.; Da Silva, M. G. C., Chemical absorption of H_2S for biogas purification. *Brazilian Journal of Chemical Engineering* **2004,** 21, (3), 415-422.
9. Yeo, Z. Y.; Chew, T. L.; Zhu, P. W.; Mohamed, A. R.; Chai, S.-P., Conventional processes and membrane technology for carbon dioxide removal from natural gas: A review. *Journal of Natural Gas Chemistry* **2012,** 21, (3), 282-298.
10. Tuinier, M. J.; van Sint Annaland, M., Biogas Purification Using Cryogenic Packed-Bed Technology. *Industrial & Engineering Chemistry Research* **2012,** 51, (15), 5552-5558.
11. Grande, C. A., Biogas Upgrading by Pressure Swing Adsorption In *Biofuel's Engineering Process Technology*, Bernardes, M. A. D. S., Ed. InTech: 2011; pp 65-84.
12. Kim, S.; Kim, J.; Moon, I., Profit optimization for bio-gas upgrading PSA process based on controlling step-time. In *Computer Aided Chemical Engineering*, 2013; Vol. 32, pp 397-402.
13. Grande, C. A.; Rodrigues, A. E., Layered vacuum pressure-swing adsorption for biogas upgrading. *Industrial and Engineering Chemistry Research* **2007,** 46, (23), 7844-7848.
14. Peter, S. A.; Baron, G. V.; Gascon, J.; Kapteijn, F.; Denayer, J. F. M., Dynamic desorption of CO_2 and CH_4 from amino-MIL-53(Al) adsorbent. *Adsorption* **2013,** 19, (6), 1235-1244.
15. Sircar, S., Separation of Methane and Carbon Dioxide Gas Mixtures by Pressure Swing Adsorption. *Separation Science and Technology* **1988,** 23, (6-7), 519-529.
16. Kim, M.-B.; Bae, Y.-S.; Choi, D.-K.; Lee, C.-H., Kinetic Separation of Landfill Gas by a Two-Bed Pressure Swing Adsorption Process Packed with Carbon Molecular Sieve: Nonisothermal Operation. *Industrial & Engineering Chemistry Research* **2006,** 45, (14), 5050-5058.

17. Yanh, R. T., *Adsorbents. Funtamentals and applications.* . John Wiley & Sons: New Jersey, 2003.
18. Cavenati, S.; Grande, C. A.; Rodrigues, A. E., Removal of carbon dioxide from natural gas by vacuum pressure swing adsorption. *Energy & Fuels* **2006,** 20, (6), 2648-2659.
19. Kapoor, A.; Yang, R. T., Kinetic separation of methane-carbon dioxide mixture by adsorption on molecular sieve carbon. *Chemical Engineering Science* **1989,** 44, (8), 1723-1733.
20. Alonso-Vicario, A.; Ochoa-Gómez, J. R.; Gil-Río, S.; Gómez-Jiménez-Aberasturi, O.; Ramírez-López, C. A.; Torrecilla-Soria, J.; Domínguez, A., Purification and upgrading of biogas by pressure swing adsorption on synthetic and natural zeolites. *Microporous and Mesoporous Materials* **2010,** 134, (1-3), 100-107.
21. Cavenati, S.; Grande, C. A.; Rodrigues, A. E., Upgrade of Methane from Landfill Gas by Pressure Swing Adsorption. *Energy & Fuels* **2005,** 19, (6), 2545-2555.
22. Cavenati, S.; Grande, C. A.; Rodrigues, A. E., Adsorption Equilibrium of Methane, Carbon Dioxide, and Nitrogen on Zeolite 13X at High Pressures. *Journal of Chemical and Engineering Data* **2004,** 49, (4), 1095-1101.
23. Leyssale, J. M.; Papadopoulos, G. K.; Theodorou, D. N., Sorption thermodynamics of CO_2, CH_4, and their mixtures in the ITQ-1 zeolite as revealed by molecular simulations. *Journal of Physical Chemistry B* **2006,** 110, (45), 22742-22753.
24. Babarao, R.; Hu, Z.; Jiang, J.; Chempath, S.; Sandler, S. I., Storage and separation of CO_2 and CH_4 in silicalite, C168 schwarzite, and IRMOF-1: A comparative study from Monte Carlo simulation. *Langmuir* **2007,** 23, (2), 659-666.
25. Bae, Y.-S.; Mulfort, K. L.; Frost, H.; Ryan, P.; Punnathanam, S.; Broadbelt, L. J.; Hupp, J. T.; Snurr, R. Q., Separation of CO_2 from CH_4 Using Mixed-Ligand Metal−Organic Frameworks. *Langmuir* **2008,** 24, (16), 8592-8598.
26. Barcia, P. S.; Bastin, L.; Hurtado, E. J.; Silva, J. A. C.; Rodrigues, A. E.; Chen, B., Single and multicomponent sorption of CO_2, CH_4 and N_2 in a microporous metal-organic framework. *Separation Science and Technology* **2008,** 43, (13), 3494-3521.
27. Liang, Z.; Marshall, M.; Chaffee, A. L., CO_2 Adsorption-Based Separation by Metal Organic Framework (Cu-BTC) versus Zeolite (13X). *Energy & Fuels* **2009,** 23, (5), 2785-2789.
28. Peng, X.; Wang, W. C.; Xue, R. S.; Shen, Z. M., Adsorption separation of CH_4/CO_2 on mesocarbon microbeads: Experiment and modeling. *AIChE Journal* **2006,** 52, (3), 994-1003.
29. Goetz, V.; Pupier, O.; Guillot, A., Carbon dioxide-methane mixture adsorption on activated carbon. *Adsorption* **2006,** 12, (1), 55-63.
30. Bazan, R. E.; Bastos-Neto, M.; Staudt, R.; Papp, H.; Azevedo, D. C. S.; Cavalcante Jr, C. L., Adsorption equilibria of natural gas components on activated carbon: Pure and mixed gas isotherms. *Adsorption Science and Technology* **2008,** 26, (5), 323-332.
31. Santos, M. P. S.; Grande, C. A.; Rodrigues, A. E., Dynamic study of the pressure swing adsorption process for biogas upgrading and its responses to feed disturbances. *Industrial & Engineering Chemistry Research* **2013,** 52, (15), 5445-5454.
32. Son, S.-J.; Choi, J.-S.; Choo, K.-Y.; Song, S.-D.; Vijayalakshmi, S.; Kim, T.-H., Development of carbon dioxide adsorbents using carbon materials prepared from coconut shell. *Korean Journal of Chemical Engineering* 22, (2), 291-297.
33. Sun, Y.; Webley, P. A., Preparation of activated carbons with large specific surface areas from biomass corncob and their adsorption equilibrium for methane, carbon dioxide, nitrogen, and hydrogen. *Industrial & Engineering Chemistry Research* **2011,** 50, (15), 9286-9294.

34. Banisheykholeslami, F.; Ghoreyshi, A. A.; Mohammadi, M.; Pirzadeh, K., Synthesis of a carbon molecular sieve from broom corn stalk via carbon deposition of methane for the selective separation of a CO_2/CH_4 mixture. *Clean - Soil, Air, Water* **2015,** 43, (7), 1084-1092.
35. Álvarez-Gutiérrez, N.; Gil, M. V.; Rubiera, F.; Pevida, C., Adsorption performance indicators for the CO_2/CH_4 separation: Application to biomass-based activated carbons. *Fuel Processing Technology* **2016,** 142, 361-369.
36. Álvarez-Gutiérrez, N.; Gil, M. V.; Rubiera, F.; Pevida, C., Cherry-stones-based activated carbons as potential adsorbents for CO_2/CH_4 separation: effect of the activation parameters. *Greenhouse Gases: Science and Technology* **2015,** 5, (6), 812-825.
37. Gil, M. V.; Álvarez-Gutiérrez, N.; Martínez, M.; Rubiera, F.; Pevida, C.; Morán, A., Carbon adsorbents for CO_2 capture from bio-hydrogen and biogas streams: Breakthrough adsorption study. *Chemical Engineering Journal* **2015,** 269, 148-158.
38. García, S.; Pis, J. J.; Rubiera, F.; Pevida, C., Predicting mixed-gas adsorption equilibria on activated carbon for precombustion CO_2 capture. *Langmuir* **2013,** 29, (20), 6042-6052.
39. García, S.; Gil, M. V.; Martín, C. F.; Pis, J. J.; Rubiera, F.; Pevida, C., Breakthrough adsorption study of a commercial activated carbon for pre-combustion CO_2 capture. *Chemical Engineering Journal* **2011,** 171, (2), 549-556.
40. Ruthven, D. M.; Farooq, S.; Knaebel, K. S., *Pressure Swing Adsorption*. VCH Publishers: New York, 1994.
41. Finsy, V.; Ma, L.; Alaerts, L.; De Vos, D. E.; Baron, G. V.; Denayer, J. F. M., Separation of CO_2/CH_4 mixtures with the MIL-53(Al) metal–organic framework. *Microporous and Mesoporous Materials* **2009,** 120, (3), 221-227.
42. Pirngruber, G. D.; Hamon, L.; Bourrelly, S.; Llewellyn, P. L.; Lenoir, E.; Guillerm, V.; Serre, C.; Devic, T., A method for screening the potential of MOFs as CO_2 adsorbents in pressure swing adsorption processes. *ChemSusChem* **2012,** 5, (4), 762-776.
43. McCabe, W. L.; Smith, J. C.; Harriott, P., *Unit operations of chemical engineering*. Seventh ed.; Mc Graw-Hill: 2005.
44. Martín, C. F.; García, S.; Beneroso, D.; Pis, J. J.; Rubiera, F.; Pevida, C., Precombustion CO_2 capture by means of phenol–formaldehyde resin-derived carbons: From equilibrium to dynamic conditions. *Separation and Purification Technology* **2012,** 98, 531-538.
45. Martín, C. F.; Stöckel, E.; Clowes, R.; Adams, D. J.; Cooper, A. I.; Pis, J. J.; Rubiera, F.; Pevida, C., Hypercrosslinked organic polymer networks as potential adsorbents for pre-combustion CO_2 capture. *Journal of Materials Chemistry* **2011,** 21, (14), 5475-5483.
46. Martín, C. F.; Plaza, M. G.; Pis, J. J.; Rubiera, F.; Pevida, C.; Centeno, T. A., On the limits of CO_2 capture capacity of carbons. *Separation and Purification Technology* **2010,** 74, (2), 225-229.
47. Wiersum, A. D.; Giovannangeli, C.; Vincent, D.; Bloch, E.; Reinsch, H.; Stock, N.; Lee, J. S.; Chang, J. S.; Llewellyn, P. L., Experimental screening of porous materials for high pressure gas adsorption and evaluation in gas separations: Application to MOFs (MIL-100 and CAU-10). *ACS Combinatorial Science* **2013,** 15, (2), 111-119.
48. Yu, H.; Wang, X.; Xu, C.; Chen, D. L.; Zhu, W.; Krishna, R., Utilizing transient breakthroughs for evaluating the potential of Kureha carbon for CO_2 capture. *Chemical Engineering Journal* **2015,** 269, 135-147.
49. Kumar, R., Pressure Swing Adsorption Process: Performance Optimum and Adsorbent Selection. *Industrial & Engineering Chemistry Research* **1994,** 33, (6), 1600-1605.

50. Krishna, R., Adsorptive separation of $CO_2/CH_4/CO$ gas mixtures at high pressures. *Microporous and Mesoporous Materials* **2012,** 156, (0), 217-223.
51. Wu, H.; Yao, K.; Zhu, Y.; Li, B.; Shi, Z.; Krishna, R.; Li, J., Cu-TDPAT, an rht-type dual-functional metal–organic framework Offering significant potential for use in H_2 and natural gas purification processes operating at high pressures. *The Journal of Physical Chemistry C* **2012,** 116, (31), 16609-16618.

610 TABLES

611 **Table 1.** Physical properties of the activated carbons

	Activated carbon		
	$CS\text{-}CO_2$	$CS\text{-}H_2O$	Calgon BPL
BET surface area ($m^2\ g^{-1}$)	1045	998	1129
Total pore volume ($cm^3\ g^{-1}$)	0.48	0.53	0.50
Micropore volume ($cm^3\ g^{-1}$)[a]	0.40	0.38	0.46
Average micropore width (nm)[b]	0.93	0.89	1.40
Narrow Micropore volume ($cm^3\ g^{-1}$)[a]	0.35	0.33	0.22
Average narrow micropore width (nm)[b]	0.78	0.74	0.70

612 [a] Evaluated with the Dubinin-Radushkevich equation.
613 [b] Determined with the Stoeckli-Ballerini relation.
614
615
616
617 **Table 2.** Characteristics of the adsorbent beds

	Activated carbon		
	$CS\text{-}CO_2$	$CS\text{-}H_2O$	Calgon BPL
Mass of adsorbent (g)	4.10	4.80	7.00
Particle size (mm)	1-3	1-3	2-4.75
Total porosity, εT	0.86	0.84	0.79
Helium density ($g\ cm^{-3}$)[a]	1.98	1.99	2.10
Apparent density ($g\ cm^{-3}$)[b]	0.53	0.64	0.83
Bed diameter (cm)	1.30	1.30	1.30
Bed height (cm)	11.55	11.65	11.90
Bed density ($g\ cm^{-3}$)	0.27	0.31	0.44

618 [a] Determined by He pycnometry.
619 [b] Determined with Hg porosimetry at 1 bar.
620
621
622

623
624 **Table 3.** Adsorbed amounts for breakthrough measurements of a simulated biogas CO_2/CH_4
625 mixture (50/50 vol. %) at 30 ºC and different pressures on CS-CO_2, CS-H_2O, and Calgon BPL.

	CO_2 adsorption capacity		CH_4 adsorption capacity	
Adsorbent	(mol kg^{-1})	(mol m^{-3})	(mol kg^{-1})	(mol m^{-3})
1 bar				
CS-CO_2	1.63	440.1	0.47	126.9
CS-H_2O	1.49	461.9	0.37	114.7
Calgon BPL	1.18	519.2	0.33	145.2
3 bar				
CS-CO_2	2.80	756.0	0.67	180.9
CS-H_2O	2.60	806.0	0.64	198.4
Calgon BPL	2.02	888.8	0.53	233.2
5 bar				
CS-CO_2	3.60	972.0	0.95	256.5
CS-H_2O	3.53	1094.3	0.76	235.6
Calgon BPL	2.70	1188.0	0.81	356.4
10 bar				
CS-CO_2	5.14	1387.8	1.55	418.5
CS-H_2O	4.48	1388.8	1.05	325.5
Calgon BPL	4.14	1821.6	1.30	572.0

626
627
628
629
630

631 FIGURES

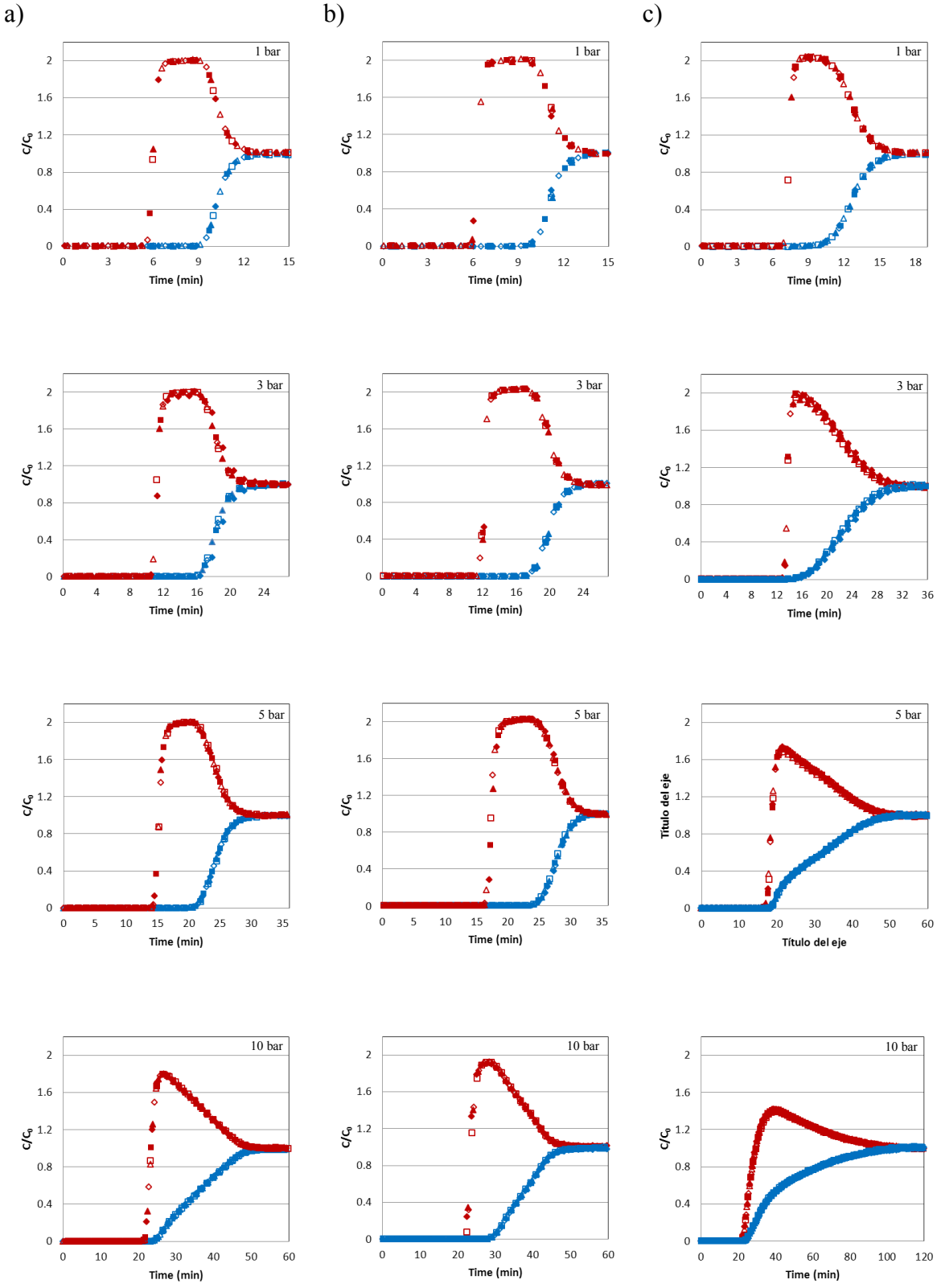

632

633 **Figure 1.** CO_2 (blue) and CH_4 (red) breakthrough curves of the experiments with CO_2/CH_4

634 mixture (50/50 vol. %) in feed gas for CS-CO_2 (a), CS-H_2O (b), and Calgon BPL (c) at 1, 3, 5,

635 and 10 bar and at 30 ºC. The six consecutive cycles are represented by the different symbols: ♦

636 cycle 1, ▲ cycle 2, ■ cycle 3, ◊ cycle 4, △ cycle 5, □ cycle 6.

637

a)

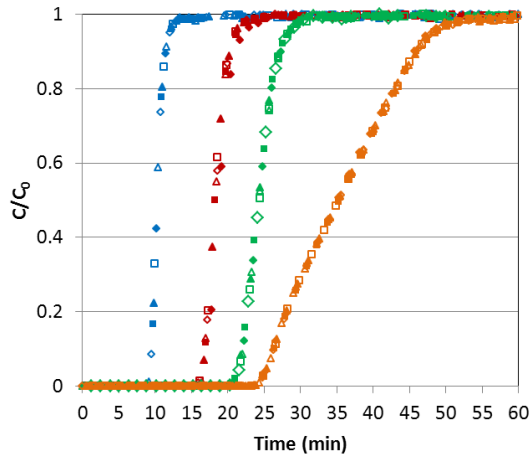
c/c0
Time (min)

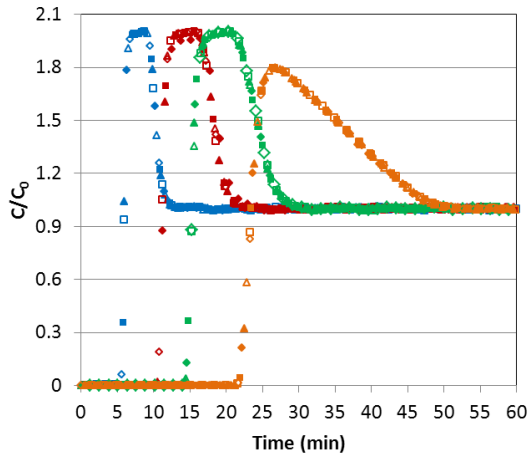
c/c0
Time (min)

b)

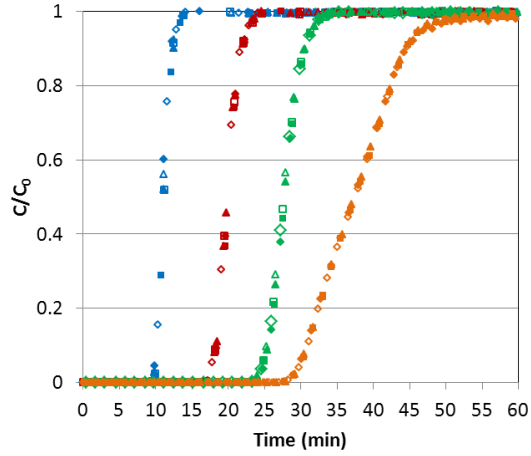
c/c0
Time (min)

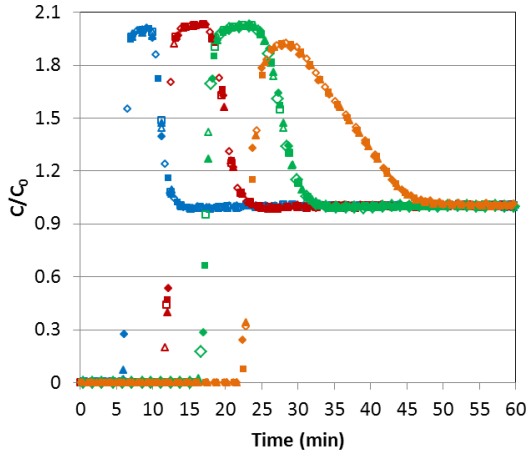
c/c0
Time (min)

c)

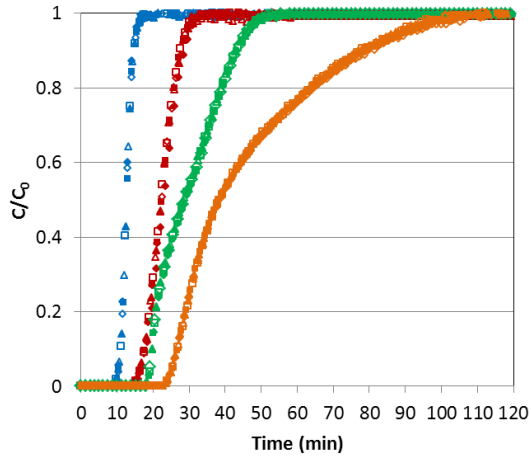
c/c0
Time (min)

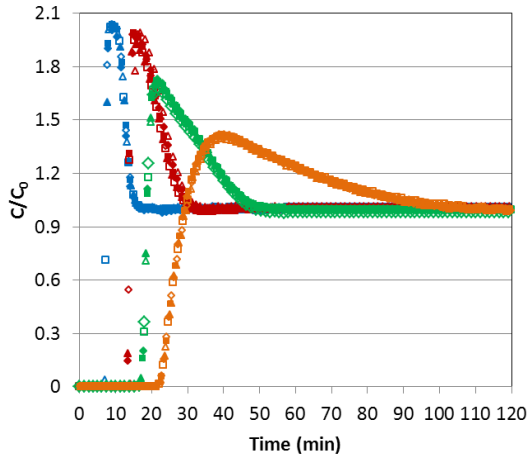
c/c0
Time (min)

d)

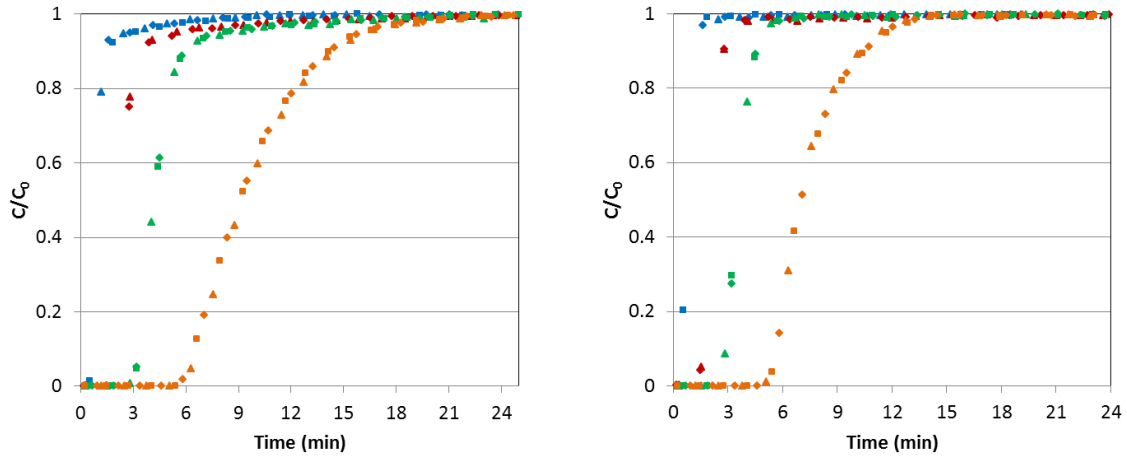

638 **Figure 2.** Comparison of CO_2 (left graphs) and CH_4 (right graphs) breakthrough curves at the
639 evaluated pressures for CS-CO_2 (a), CS-H_2O (b), Calgon BPL (c) and Blank experiments (d). 1
640 bar (blue), 3 bar (red), 5 bar (green), 10 bar (orange). Feed: CO_2/CH_4 mixture (50/50 vol. %) at
641 30 ºC.
642

643

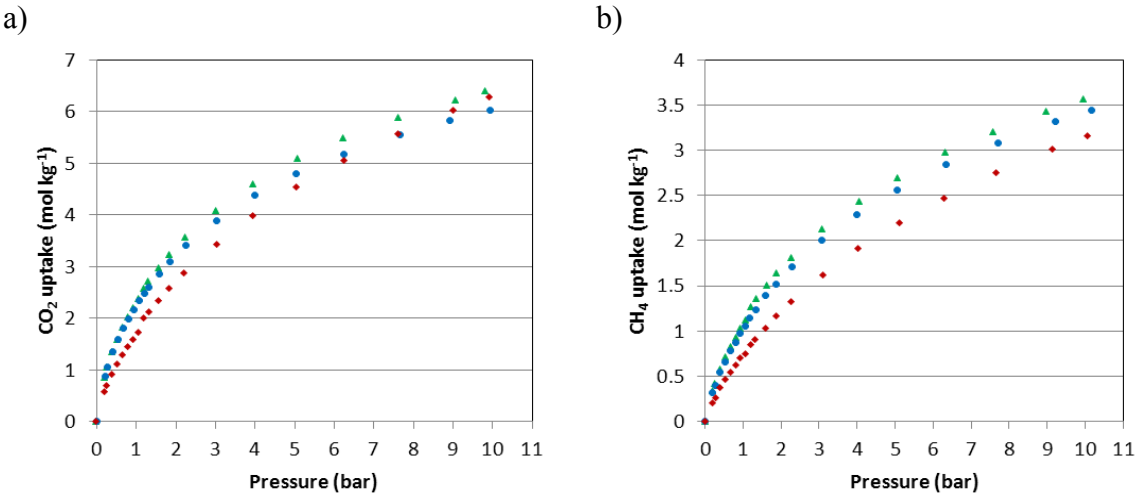

644 **Figure 3.** Adsorption isotherms at 30 ºC and up to 10 bar of CO_2 (a) and CH_4 (b) on CS-CO_2

645 (green colour), CS-H_2O (blue colour), and Calgon-BPL (red colour).

646

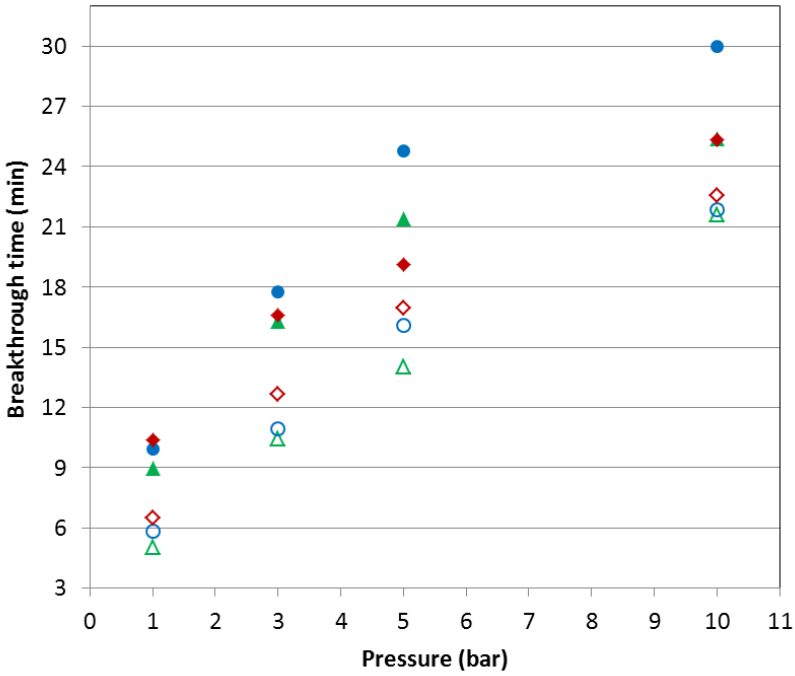

Figure 4. CO_2 (full symbols) and CH_4 (open symbols) breakthrough timesas a function of pressure: CS-CO_2 (green colour), CS-H_2O (blue colour), and Calgon BPL (red colour). Feed: CO_2/CH_4 mixture (50/50 vol. %) at 30 ºC.

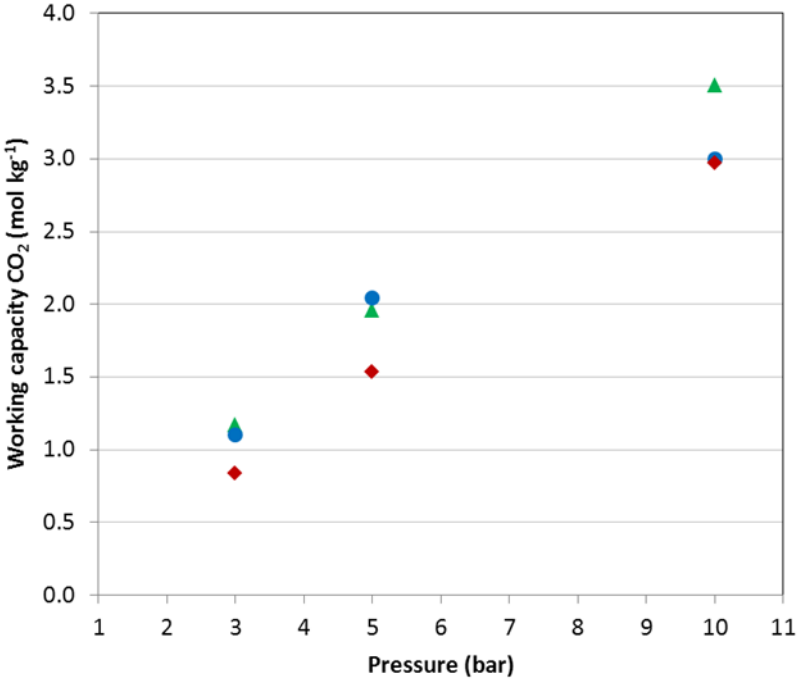

Figure 5. Working capacity of CO_2 as a function of pressure for CS-CO_2 (green colour), CS-H_2O (blue colour), and Calgon BPL (red colour). Values estimated from binary breakthrough tests.

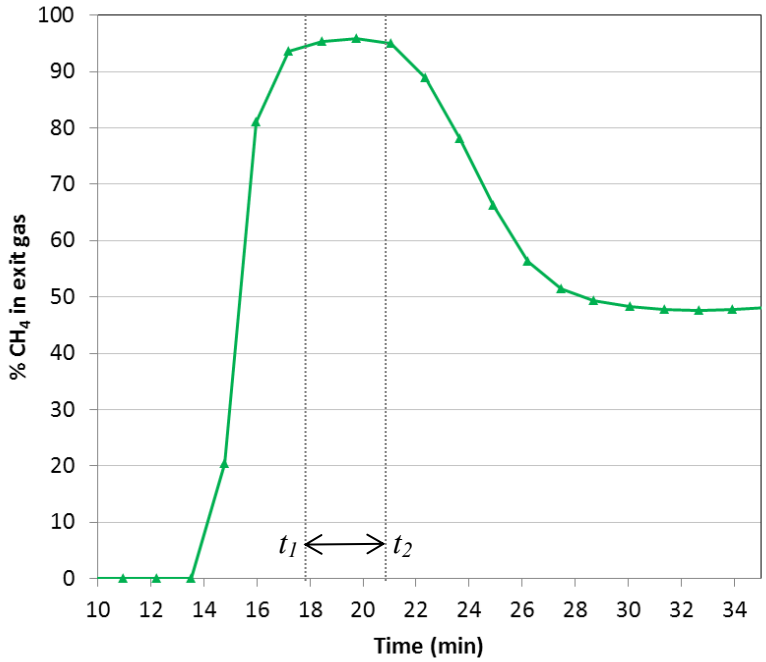

Figure 6. CH_4 breakthrough for CO_2/CH_4 mixture (50/50 vol. %) at 30 ºC and at 5 bar in the fixed bed packed with CS-CO_2.

662

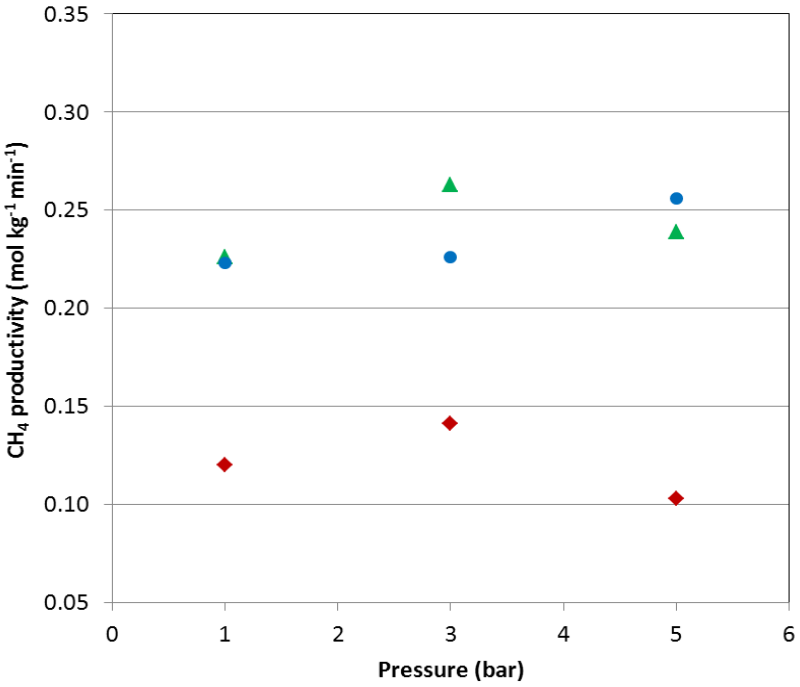

663 **Figure 7.** CH_4 productivity versus pressure for CS-CO_2 (green symbols), CS-H_2O (blue
664 symbols), and Calgon BPL (red symbols). Values estimated from binary breakthrough tests
665 (section 3.1). Note: t_1 and t_2 were selected for each adsorbent at each pressure according to the
666 criteria of maximum CH_4 purity in the outlet gas stream.

667

668

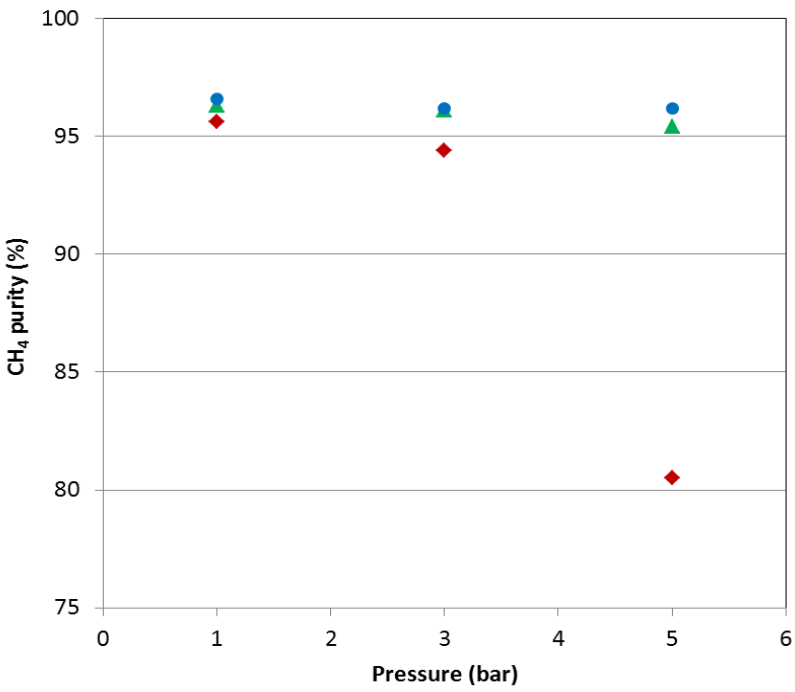

669

670 **Figure 8.** Purity of CH_4 in the outlet gas stream as a function of pressure for CS-CO_2 (green

671 symbols), CS-H_2O (blue symbols), and Calgon BPL (red symbols). Values estimated from

672 binary breakthrough tests.

673

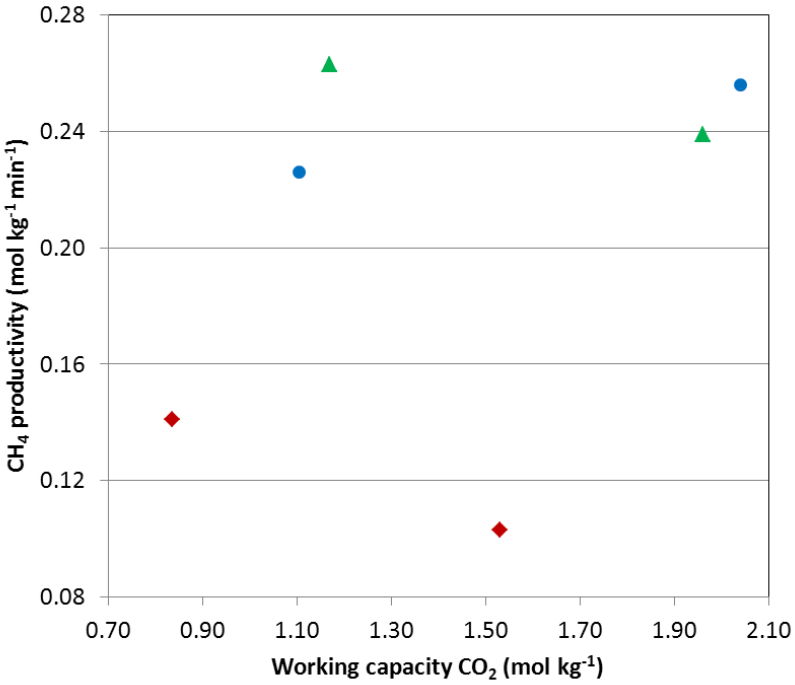

Figure 9. Productivity of CH_4 versus the CO_2 working capacity for CS-CO_2 (green symbols), CS-H_2O (blue symbols), and Calgon BPL (red symbols). Values estimated from binary breakthrough tests.